NANO LETTERS

2007
Vol. 7, No. 12
3669−3674

Quantitative Three-Dimensional Reconstruction of Catalyst Particles for Bamboo-like Carbon Nanotubes

Sara Bals,*,† K. Joost Batenburg,‡ Jo Verbeeck,† Jan Sijbers,‡ and Gustaaf Van Tendeloo†

EMAT, University of Antwerp, Groenenborgerlaan 171 B-2020 Antwerp, Belgium, and Vision Lab, University of Antwerp, Universiteitsplein 1 B-2610 Wilrijk, Belgium

Received August 3, 2007; Revised Manuscript Received October 13, 2007

ABSTRACT

The three-dimensional (3D) structure and chemical composition of bamboo-like carbon nanotubes including the catalyst particles that are used during their growth are studied by discrete electron tomography in combination with energy-filtered transmission electron microscopy. It is found that cavities are present in the catalyst particles. Furthermore, only a small percentage of the catalyst particles consist of pure Cu, since a large volume fraction of the particles is oxidized to Cu_2O. These volume fractions are determined quantitatively from 3D reconstructions obtained by discrete tomography.

Introduction. Depending on the preparation method, carbon nanotubes appear in different varieties. One of these, the so-called bamboo-like carbon nanotubes, yields hollow compartments. The growth of bamboo-like carbon nanotubes has been the subject of numerous studies.[1−5] Although the exact growth mechanism remains unclear, it has been found that the catalyst nanoparticles used during the growth of such nanotubes play a crucial role.[6] The composition of the particle determines the catalytic activity for decomposition of the carbon compounds, and it is suggested that the diameter of the carbon nanotube is affected by the size of the particle as well. Therefore, it is important to investigate the catalyst particles from both a structural as well as chemical point of view, preferably in a quantitative manner. Transmission electron microscopy (TEM) is well suited for this purpose, but the technique *only* provides a two-dimensional (2D) projection of a three-dimensional (3D) object. This problem can be overcome by combining TEM with tomography. Electron tomography basically consists of three steps: acquisition of a tilt series of projections, alignment of the projections, and 3D reconstruction. For the acquisition, different TEM techniques such as bright field TEM,[7] high angle annular dark field scanning TEM (HAADF-STEM),[8] annular dark field TEM,[9] and energy-filtered TEM (EFTEM)[8] can be used. Alignment is usually done using cross-correlation or tracking of fiducial Au markers. For the final reconstruction, different algorithms are available as well: besides weighted back-projection,[10,11] one can use iterative procedures such as the simultaneous iterative reconstruction technique (SIRT)[12] and the algebraic reconstruction technique (ART).[12,13] None of these techniques uses prior knowledge on the object that has to be reconstructed. Therefore, a large number of projections are required to obtain a reconstruction of reasonable accuracy. Moreover, the quality of the reconstructions is severely limited by the presence of so-called missing wedge artifacts, which will be further discussed in the Experimental Section. These artifacts will have a major influence on the ability of obtaining quantitative information in three dimensions. In order to interpret the 3D reconstructed volume, one has to visualize the results. In the case of a quantitative interpretation, an additional segmentation step is required to determine the correspondence between different grayscales in the reconstruction and different compositions in the original structure. Even if projection images could be acquired from a full range of angles, several other types of artifacts will hamper this segmentation step. A quantitative interpretation based on the conventional reconstruction algorithms is therefore quite difficult and can be unreliable.

In this study, we have used discrete tomography, a technique that has been recently applied to electron tomography for the first time.[14] It will be shown that the quality of the discrete reconstruction is better in comparison to conventional reconstruction techniques. Missing wedge artifacts are strongly reduced, and, furthermore, segmentation is performed automatically during the reconstruction proce-

* Corresponding author. E-mail: Sara.Bals@ua.ac.be.
† EMAT.
‡ Vision Lab.

10.1021/nl071899m CCC: $37.00
Published on Web 11/14/2007

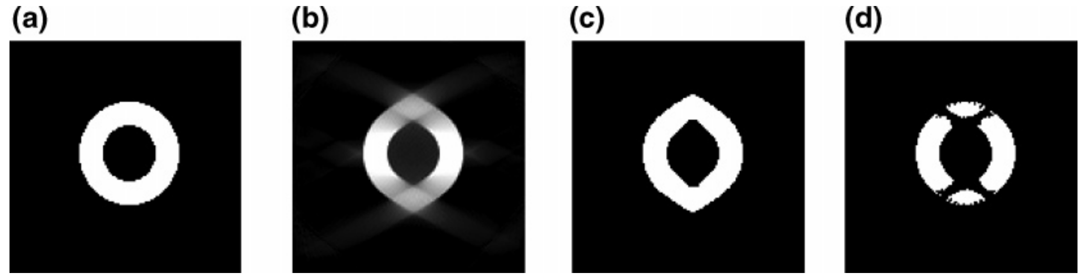

Figure 1. (a) Simulated 2D cross-section image of a 3D tubule, aligned in the same direction as the tilt axis of the microscope. (b) SIRT reconstruction from simulated projections between −60° and +60°, using perfect, noiseless projection data. (c) Thresholded SIRT reconstruction, using a low threshold. The shape of the reconstruction is clearly different from the original image. (d) Thresholded SIRT reconstruction, using a high threshold. The shape of the reconstruction is circular, but holes appear in the reconstructed tubule.

dure. This will allow us to obtain quantitative results, where the contents of each voxel is directly linked to a specific composition in the sample. By combining our 3D reconstruction with EFTEM results, we can completely describe the 3D structure and chemical composition of the catalyst particles in a quantitative manner. This information is of crucial importance to understand and optimize the growth of carbon nanotubes.

Experimental Section. In this study, carbon nanotubes have been grown by chemical vapor deposition starting from alkali-element-modified Cu/MgO catalysts, prepared by a sol−gel method. More details on the growth can be found in ref 15.

In order to obtain 3D information, an HAADF-STEM tilt series of a single carbon nanotube is acquired on a Titan 80-300 microscope (FEI) using a Fischione ultrahigh-tilt tomography holder. This results in an angular range of −54 to +74°, with projections taken every 2°. To obtain 3D information from the acquired tilt series, Inspec3D is used to align the 2D projections of the HAADF-STEM tilt series. 3D reconstruction was carried out using our own implementation of the SIRT algorithm as well as using discrete reconstruction. Details on the SIRT algorithm are presented in ref 12, whereas the use of discrete tomography is explained in more detail below.

Artifacts. Because of the inability to tilt the sample over the full 180 degrees, projection data cannot be recorded for a range of angles. To understand the limitations imposed by this problem, we must consider the Fourier transform of the reconstructed image. For each cross-section through the volume, orthogonal to the tilt-axis, the relation between the one-dimensional Fourier transform of the measured projection data and the 2D Fourier transform of the cross-section image is determined by the Fourier slice theorem (section 3.2 in ref 16). The lack of projections for a range of angles results in a "missing wedge" of information in Fourier space. When a reconstruction is computed using continuous methods such as weighted back-projection or SIRT, the lack of available projection data causes artifacts, as illustrated in Figure 1. Figure 1a shows a simulated 2D cross-section of a 3D tubule, for which the projections have been computed at 1° intervals between −60° and +60°. Figure 1b shows the SIRT reconstruction from the simulated projection data. Note that, although the test object in Figure 1a is homogeneous, the reconstructed tubule is not homogeneous at all. Moreover, the boundaries of the reconstruction extend well beyond the boundaries of the original object. This makes it very difficult, or even impossible, to obtain a quantitative measure of the size and shape of the object based on the reconstruction. Such effects become even more profound if the object of interest contains holes or has a varying composition. To obtain quantitative information from the reconstruction, the reconstructed volume is typically segmented by thresholding. Figure 1c,d shows the result of thresholding the SIRT reconstruction at different threshold levels. It is clear that the missing range of projection angles can lead to erroneous estimations of both shape and volume of the structure of interest.

The artifacts that are the result of the missing wedge of acquisition angles are usually called "missing wedge artifacts", or "fanning artifacts". One of the properties of missing wedge artifacts is that image features are elongated in the direction of the 0° beam angle. Note that, because of the missing wedge, there is no longer a *unique* reconstruction. The part of the Fourier transform of the reconstruction that lies inside the missing wedge can take any value, independent of the measured projections. One should therefore be very cautious in interpreting the results.

We remark that it is usually quite easy to hide missing wedge artifacts by displaying the 3D reconstruction from an angle close to the electron beam orientation. The artifacts are most clearly visible when viewing the reconstruction *orthogonal* to the beam orientation, as this is the direction where there is a lack of information. Although changing the display angle can help to obtain an adequate visualization, it does not alleviate the problems encountered in segmenting the reconstructed volume.

Discrete Tomography. Discrete tomography is a new reconstruction technique that can be used to reconstruct samples that consist of only a few different materials. Ideally, each of the materials should correspond to a unique gray level in the reconstruction. The basic idea of discrete tomography is to exploit this property as prior knowledge in the reconstruction algorithm. In addition to the measured projection data, the algorithm takes the set of possible gray levels as an additional reconstruction parameter. It then

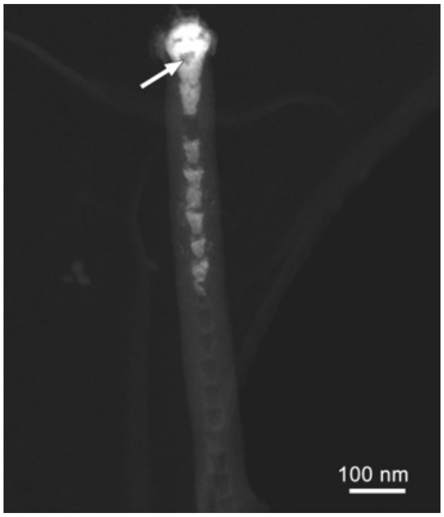

Figure 2. HAADF-STEM image from the acquired tilt series showing the catalyst particle and the bamboo-like carbon nanotube. The catalyst material is partially filling the hollow compartments. The arrow indicates an area in the catalyst particle that may correspond to a thinner area or an area with different chemical composition.

computes a reconstruction that has only gray levels from the given set, and still corresponds well with the projection data. Although it may still happen that the reconstruction is not unique, it is often possible to compute an accurate discrete reconstruction even in case of a missing wedge of angles. Recently, a new discrete reconstruction algorithm was developed that is robust and efficient, and can be used on large 3D datasets.[17,18] This algorithm, called DART, was used to compute a discrete reconstruction from our experimental dataset.

Results. A 2D image from the tilt series is presented in Figure 2. The bamboo structure of the carbon nanotube as well as the catalyst particle can be clearly distinguished. Furthermore, it can be seen that the catalyst material is also filling some of the hollow compartments of the carbon nanotube. The reason for using HAADF-STEM rather than conventional bright field TEM is that diffraction contrast present in bright field TEM images is expected to result in additional artifacts in the 3D reconstruction. Furthermore, HAADF-STEM yields structural as well as chemical information since the intensity present in an image depends on the atomic number Z. Besides chemical composition, the intensity is also determined by thickness. When investigating Figure 2, it is clear that the area in the catalyst particle marked by the arrow shows less intensity. However, from a single 2D image, it is not possible to conclude whether this area corresponds to an area with different composition or to an area with lower thickness, for example, corresponding to a cavity. Even if one would be able to conclude that the lower gray level is due to a smaller thickness, it still can not be concluded whether a cavity is present or whether material is lacking at the surface of the particle. This clearly shows the need for 3D imaging techniques.

3D reconstructions are made using SIRT as well as using DART. The results are shown in Figures 3 and 4, in which three orthogonal slices through the 3D reconstructed volume

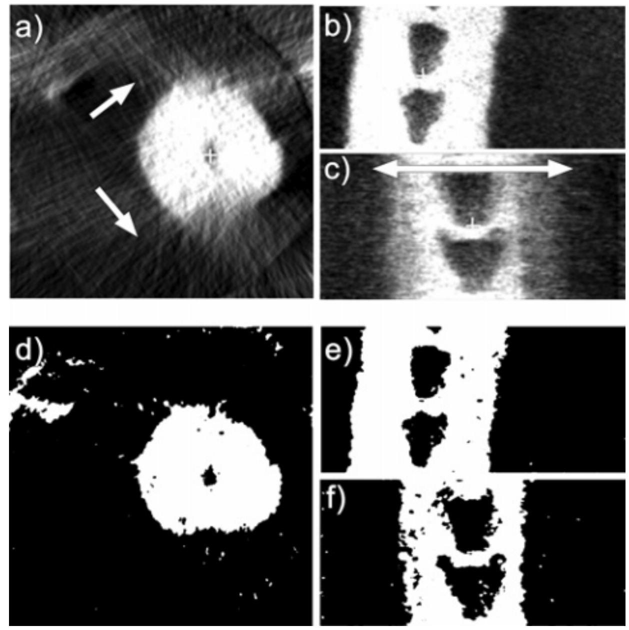

Figure 3. (a−c) Three orthogonal slices through the carbon nanotube as reconstructed by SIRT. (d−f) The corresponding slices obtained by discrete tomography. Artifacts due to the missing wedge (fanning artifacts and elongation) are indicated by arrows in panels a and c.

are presented. The images in Figure 3, where the reconstruction is focused on the lower part of the carbon nanotube, suggest that the reconstruction based on DART has better quality. Fanning artifacts that appear in the SIRT reconstruction because of the missing wedge are indicated by arrows in Figure 3a. These artifacts are strongly reduced in the DART reconstruction, as can be seen in Figure 3d. Also, the elongation (marked by the white arrow) that can be observed in Figure 3c is a result of the missing wedge, and, again, this artifact can be reduced using discrete tomography. In Figure 4, 3D reconstructions of the catalyst particle present at the top of the carbon nanotube are presented. By comparing the SIRT and the DART reconstruction, the advantages of using discrete tomography rather than SIRT are again obvious.

During the preparation of the catalyst, it is expected that Cu particles form.[15] Initially, it was assumed that the top of the catalyst consists only of Cu. Therefore, a DART reconstruction is computed using only two gray levels, for the background and the Cu, respectively. The resulting reconstruction does not correspond well with the measured projection data, which suggests that more than two gray levels should be used. The fact that more than two gray levels must be used can also be concluded by looking at an intermediate reconstruction computed by DART. Each iteration of DART consists of a continuous reconstruction step, resulting in an image that contains many gray levels, followed by a discretization step, resulting in a discrete image. If only two gray levels are used, the intermediate continuous reconstruction keeps moving away from the discrete reconstruction in each iteration, as shown in Figure 4d,e,f.

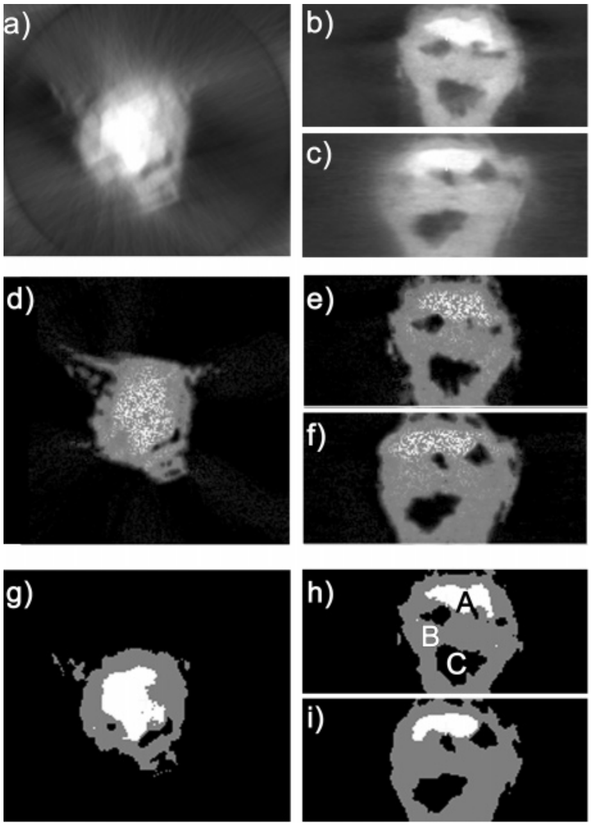

Figure 4. (a−c) Three orthogonal slices through the catalytic nanoparticle as reconstructed by SIRT (d−f) Intermediate continuous results of DART, using only two gray levels. From these images, it is clear that a third gray level should be used. (g−i) The final DART reconstruction using three gray levels. In panel h, areas with different grayscale and possibly different composition are labeled A, B, and C.

When a third gray level is added (see Figure 4g,h,i), a reconstruction is obtained that corresponds well with the measured projection data. That is, if we simulate the projections of the reconstructed structure, the simulated projection data corresponds properly with the experimental dataset.

In both the SIRT and DART reconstructions, it is obvious that the reconstructed catalyst particle is not homogeneous. Different grayscale values (labeled A, B, and C in Figure 4h) are present inside the particle, suggesting that these areas have a different density and, therefore, different compositions. The intensity of C (corresponding to the darker areas shown in Figure 2) is comparable to the intensity of the vacuum surrounding the carbon nanotube, suggesting that cavities are present inside the particle. When inspecting the aligned tilt series (see additional info), it must be noted that residual diffraction contrast can be observed throughout the complete catalytic material. This is particularly noticeable for area A, where the diffraction contrast can be observed as a sudden change in the intensity when a zone axis for this part of the catalyst particle is reached during the acquisition of the tilt series. As mentioned before, diffraction contrast is strongly suppressed as a result of the integration of the signal over a wide angular detector, but residual diffraction contrast remains possible unless the detector

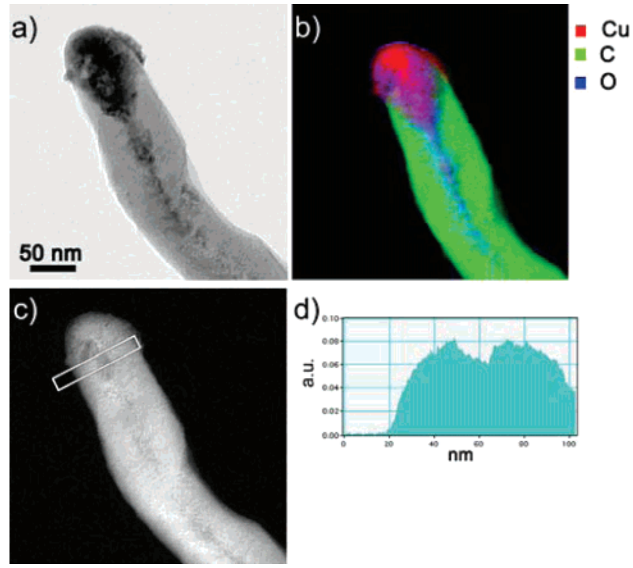

Figure 5. (a) Bright field TEM image of a bamboo-like carbon nanotube, (b) the corresponding EFTEM colormap, and (c) the EFTEM thickness map. (d) An intensity profile along the direction indicated in panel c suggesting a decrease in thickness.

covers the whole diffraction plane. To investigate whether the presence of the remaining diffraction contrast may explain the different grayscale values found in Figure 4, a second reconstruction using DART has been carried out, excluding the 2D projections in which apparent diffraction contrast is present. This means that nine projections have been removed from the data set. Nevertheless, the resulting DART reconstruction does not show any remarkable difference in comparison to the reconstruction based on all 2D projections. This proves that the difference in grayscale value is indeed due to the presence of different densities and that the possibility of diffraction contrast can be ruled out.

In order to identify these different chemical compositions, EFTEM elemental maps have been acquired. An example of a colormap, obtained using the three-window elemental mapping technique,[19] is shown in Figure 5b. The EFTEM map clearly confirms the observations made by electron tomography; that is, different compositions are present inside the catalytic particle. In Figure 5b, it can be seen that the top part of the catalyst consists of Cu only, whereas the majority of the particle has a Cu_2O composition. The stoichiometric ratio between Cu and O was determined from calculated *k*-factors based on hydrogenic cross-sections integrated in an energy width equal to the experimental energy selecting slit.[19] Different regions in different nanotubes were found to consist of either metallic Cu or Cu_2O, and no indication of the presence of CuO was found. Therefore, it can be concluded that the brightest areas in Figure 4 consist of Cu, whereas the gray areas correspond to Cu_2O. It is important to note that the catalytic material filling up the bamboo-like compartments also has a Cu_2O composition. Furthermore, it is obvious that the catalyst particle is not encapsulated by the C.

In order to investigate the presence of holes inside the catalyst particles, an EFTEM thickness map (Figure 5c with

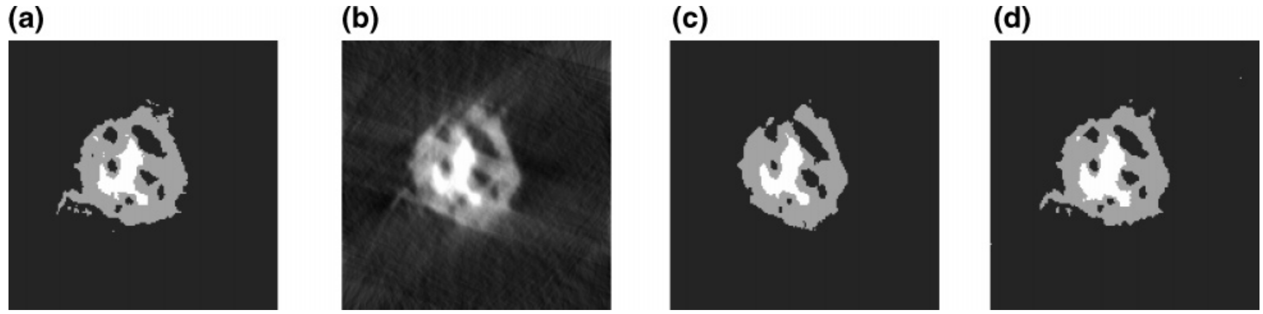

Figure 6. (a) Simulated 2D cross-section image of the top part of the catalyst. (b) SIRT reconstruction from simulated projections between $-54°$ and $+74°$, where noise and a small misalignment has been applied to each projection image. (c) Thresholded SIRT reconstruction. (d) DART reconstruction, from the same noisy projection data.

the corresponding intensity profile in Figure 5d) is obtained as well. This is done using the log-ratio method.[19] In this procedure, an energy-loss spectrum is recorded, and the integrated area I_0 under the zero-loss peak is compared to the total area I_t under the whole spectrum. The sample thickness t is given by

$$t/\lambda = \ln(I_t/I_0)$$

with λ being the mean free path for all inelastic scattering. The thickness profile presented in Figure 5d was taken along the direction indicated in Figure 5c. The profile shows a decrease in intensity corresponding to a lower thickness. Combining this observation with the results previously found by tomography allows us to conclude that cavities are indeed present inside the catalyst particle.

Besides the fact that DART yields reconstructions with a better quality, a major advantage of the technique is that it allows one to quantify the observations in a straightforward way since the reconstruction is already segmented. This is in contrast to SIRT reconstructions, which often have to be segmented in a manual and therefore subjective way. Obviously, the fact that DART yields a segmented reconstruction is a major advantage when one wants to obtain quantitative information in three dimensions. However, the question can be raised whether the segmentation is reliable. Therefore, we have investigated whether the quality of the discrete reconstruction suffers from the missing wedge. In a simulation study, the output of the DART algorithm, based on the experimental tilt series, is reprojected to form artificial, noiseless projection data along the same projection angles as those used in the real experiment. To make the simulation more realistic, Gaussian noise is added to each of the projection images, and each of the projection images is misaligned by a small, random amount of, at most, one detector pixel. The resulting projections are used as input for a new SIRT and DART reconstruction. Note that the discrete reconstruction consists of three gray levels, corresponding to the background, the Cu, and the Cu_2O. Figure 6a shows the simulated test object that is used to generate the projection data. The SIRT and DART reconstructions are shown in Figure 6, panels b and d, respectively. The results show clearly that the SIRT reconstruction is of substantially lower quality than the discrete reconstruction. Figure 6c shows the SIRT reconstruction after thresholding has been applied to segment the reconstruction. Both the shape and the total volume of the Cu and Cu_2O regions are different from the phantom, whereas, for the discrete reconstruction, the Cu and Cu_2O areas match the original object almost perfectly. These results allow us to conclude that our experimental results are reliable and can therefore be used for quantitative analysis. On the basis of the DART reconstruction of the experimental tilt series, the total volume of each of the different chemical compositions can now be determined in a straightforward manner, by counting the number of voxels corresponding to each gray value. This approach has been used to analyze the composition of the tip of the catalytic compound (see Figure 4). It is found that the total volume of the area presented in Figure 4 consists of 210 220 voxels, of which 179 430 voxels belong to the Cu_2O part, 11 780 belong to Cu, and 19 010 belong to the hollow parts. This corresponds to an 85% composition of Cu_2O and 6% of Cu, whereas 9% of the particle is expected to be hollow. Although a 2D study (e.g., a single EFTEM map) would be able to give some information on the composition of the particle, it is only by combining this with 3D information obtained by discrete tomography that one is able to obtain quantitative information in three dimensions.

Discussion. Using discrete tomography, we have studied the shape of bamboo-like carbon nanotubes. As is shown in Figure 3, the hollow compartments in the nanotubes have a cone-like 3D structure. This structure resembles the lower part of the catalytic nanoparticle, suggesting that, during growth, graphite sheets nucleate around the bottom of the catalyst nanoparticle. In situ TEM experiments presented in ref 20 show a similar process for tip-growth of bamboo-like carbon nanotubes using Ni as a catalyst. During growth, the Ni particles elongate to a similar cone-like shape as observed in this study. The in situ experiments furthermore show that, as the growth of the nanotube proceeds, the Ni particles will retract, yielding a new hollow compartment. Our results suggest a similar mechanism, although, in this case, hollow compartments as well as situations where the catalyst material is surrounded by the graphite sheets and incorporated inside the carbon nanotube during growth are likely to occur.

In this study, special attention is devoted to the (inner) structure and chemical composition of the catalyst particles used during the growth of carbon nanotubes. Our results show that the composition of the nanoparticle is not uniform. Only a small percentage of the particles consist of pure Cu, and a large volume fraction of the particle is oxidized to Cu_2O. It is important to know whether Cu_2O was formed before or after growth of the carbon nanotubes. In previous studies,[15] it was expected that the carbon nanotubes grow on Cu particles, which are reduced from CuO, on a MgO substrate. It might be possible that the oxidation to Cu_2O occurs when the carbon nanotubes and the catalyst particles are exposed to air after growth. However, Cu_2O is present in the compartments of the carbon nanotubes as well, and this suggests that oxidation after growth is less likely, since it has been shown recently that a carbon coating is very efficient when preventing oxidation of Cu.[21] The possibility that Cu_2O rather than Cu is present during the growth of carbon nanotubes is an interesting observation. Co and Ni are mostly used as catalysts during the growth of carbon nanotubes since these transition metals have non-filled d shells and are therefore able to interact with hydrocarbons during growth.[6] Cu, however, is a non-transition metal with its 3d shell completely filled, and it was observed to yield only amorphous carbon during an attempted growth of carbon nanotubes.[22] In Cu_2O, on the other hand, d-orbital holes have been observed.[23] During growth of the carbon nanotubes in this study, alkali-elements (K) were used to induce growth of the nanotubes.[15] At present, it is not clear which effect, that is, the presence of Cu_2O or the presence of K, is responsible for the growth of the carbon nanotubes, and further studies have to be carried out. In this respect, it must be noted that Raman studies have indicated a strong interaction between Cu_2O and the multiwalled carbon nanotubes on which they were deposited.[24]

An interesting observation that can be made from the 3D reconstructions as well is the presence of voids in the nanoparticle. A possible explanation for these cavities can be found by careful inspection of the tilt series presented as Supporting Information. In this series, diffraction contrast can be observed as a sudden change in the intensity when a zone axis is reached during the acquisition of the tilt series. Different areas of the catalytic material show this change in intensity at different projection angles, which suggests that the catalytic material is polycrystalline. Therefore, the catalytic material can be regarded as a nanocluster rather than a single-crystalline nanoparticle. In such agglomerates, cavities are likely to appear when the individual parts of the nanoclusters do not coalescence.

Conclusions. In conclusion, the inner structure and composition of the catalytic particles used during the growth of bamboo-like carbon nanotubes has been studied quantitatively in three dimensions. This information is of great importance when trying to understand the growth of carbon nanotubes using catalysts. By using HAADF-STEM tomography, we have been able to conclude that different compositions are present inside the catalyst particle. By EFTEM maps, we are able to identify these different compositions as Cu and Cu_2O. EFTEM furthermore confirms the presence of cavities, as suggested by the electron tomography results. Finally, it has been shown that DART results in a reliable segmentation, which allows one to obtain quantitative information in a straightforward manner.

Acknowledgment. The authors acknowledge financial support from the European Union under the Framework 6 program under a contract for an Integrated Infrastructure Initiative. (Reference 026019 ESTEEM). S.B., K.B., and J.S. are grateful to the Fund for Scientific Research-Flanders (Contract No. G.0247.08). This work has been performed within the Interuniversity Attraction Poles Programme, Belgian State, Belgian Science Policy. This study would have been impossible without the help of E. Sourty at FEI. The authors also thank Prof. X. Zhang and Dr. X. Tao for provision of the sample and useful discussions.

Supporting Information Available: A movie is provided as Supporting Information, presenting the aligned tilt series of HAADF-STEM images. This material is available free of charge via the Internet at http://pubs.acs.org.

References

(1) Li, D. C.; Dai, L. M. *Chem. Phys. Lett.* **2000**, *316*, 349.
(2) Li, Y. D.; Chen, J. L. *Chem. Commun.* **1999**, *12*, 1141.
(3) He, C.; Naiqin, Z.; Shi, C.; Du, X.; Li, J. *J. Alloys Compd.* **2007**, *433*, 79.
(4) Chen, X.; Wang, R.; Xu, J.; Dapeng, Y. *Micron* **2004**, *35*, 455.
(5) Lin, M.; Tan, J.; Boothroyd, C.; Loh, K.; Tok, E.; Foo, Y.-L. *Nano Lett.* **2007**, *7*, 2234.
(6) Dupuis, A.-C. *Prog. Mater. Sci.* **2005**, *50*, 929.
(7) Koster, A. J.; Ziese, U.; Verkleij, A. J.; Janssen, A. H.; de Jong, K. P. *J. Phys. Chem. B* **2000**, *104*, 9368.
(8) Midgley, P. A.; Weyland, M. *Ultramicroscopy* **2003**, *96*, 413.
(9) Bals, S.; Van Tendeloo, G.; Kisielowski, C. *Adv. Mater.* **2006**, *18*, 892.
(10) Crowther, R. A.; de Rosier, D. J.; Klug, A. *Proc. R. Soc. London, Ser. A* **1970**, *317*, 319.
(11) Gilbert, P. F. C. *Proc. R. Soc. London, Ser. B* **1972**, *182*, 89.
(12) Gordon, R.; Bender, R.; Herman, G. T. *J. Theor. Biol.* **1970**, *29*, 471.
(13) Gilbert, P. *J. Theor. Biol.* **1972**, *36*, 105
(14) Batenburg, K. J.; Bals, S.; Sijbers, J.; Kaiser, U.; Kuebel, C.; Kisielowski, C.; Gomez, E. *Ultramicroscopy*, to be submitted for publication.
(15) Tao, X.; Zhang, X.; Cheng, J.; Wang, Y.; Liu, F.; Luo, Z. *Chem. Phys. Lett.* **2005**, *409*, 89.
(16) Kak, A. C.; Slaney, M.: *Principles of Computerized Tomographic Imaging*; Society for Industrial and Applied Mathematics: Philadelphia, PA, 2001.
(17) Batenburg, K. J.; Sijbers, J. DART: A fast heuristic algebraic reconstruction algorithm for discrete tomography. Proceedings of the IEEE International Conference on Image Processing, San Antonio, Texas, September 16−19, 2007; TP-L5.2.
(18) Batenburg, K. J.; Sijbers, J. *IEEE Trans. Image Process.*, to be submitted for publication.
(19) Egerton, R. F. *Electron Energy-Loss Spectroscopy in the Electron Microscope*, 2nd ed.; Plenum Publishing Corp.: New York, 1996.
(20) Lin, M.; Tan, J. P. Y.; Boothroyd, C.; Loh, K. P.; Tok, E. S.; Foo, Y.-L. *Nano Lett.* **2007**, *7*, 2234.
(21) Zhang, X. F.; Dong, X. L.; Huang, H.; Wang, D. K.; Lv, B.; Lei, J. P. *Nanotechnology* **2007**, *18*, 275701.
(22) Ivanon, V.; Nagy, J. B.; Lambin, P.; Lucas, A.; Zhang, X. F.; Bernaerts, D. *Chem. Phys. Lett.* **1994**, *223*, 329.
(23) Zuo, J. M.; Kim, M.; O'Keeffe, M.; Spence, J. H. *Nature* **1999**, *401*, 49.
(24) Yu, I.; Ma, L.-L.; Huang, W.-Y.; Du, F.-P.; Yu, J. C.; Yu J.-G.; Wang, J.-B.; Wong, P.-K. *Carbon* **2005**, *43*, 651.

NL071899M